

A perfect pair: Niobium- and gallium-doped ceramic biomaterial enabled by coupled synthesis method with potential application for bone regeneration and cancer-targeted therapy

Guilherme S. Medeiros^{1,2}, Luis F. M. Oliveira¹, Filipe V. Ferreira⁴, Lucas P. Souza³, Richard A. Martin³, Ivone R. de Oliveira⁵, João H. Lopes^{1}*

¹Department of Chemistry, Division of Fundamental Sciences (IEF), Aeronautics Institute of Technology - ITA, 12228-900, São José dos Campos-SP – Brazil. ³College of Engineering and Physical Sciences, Aston University, B47ET Birmingham – United Kingdom. ⁴Nanotechnology National Laboratory for Agriculture (LNNA), Embrapa Instrumentation, 13560-979, São Carlos, SP – Brazil. ⁵University of Vale do Paraíba (UNIVAP). Research and Development Institute (IP&D), 12244-390, São José dos Campos-SP – Brazil.

***Corresponding author**

Prof. João H. Lopes. Department of Chemistry, Division of Fundamental Sciences (IEF), Aeronautics Institute of Technology - ITA, 12228-900, Sao Jose dos Campos-SP – Brazil.

E-mail: lopes@ita.br

Abstract

In this work, we report the synthesis and characterization of sol-gel bioactive glasses containing niobium (Nb) and gallium (Ga), aiming at a multifunctional glass that synergistically combines the respective effects of these species in potentiating bone repair and regeneration, concomitantly with a bone cancer targeted therapy. We found that the entry of Ga^{3+} into the vitreous network promotes an increase in the network connectivity, contributing to an increase in the degree of polymerization of the glass, since part of the calcium ions that behave as network modifying agents were replaced by gallium ions that act as network formers, and hence a replacement of part of the $\text{Si-O}\cdots\text{Ca}^{2+}\cdots\text{O-Si}$ by Si-O-Ga-O-Si bonds. Such results confirmed an increase in bridging oxygen bond density associated with a decrease in the number of bonds per unit volume of the glass due to the expansion of the glassy network. Furthermore, the incorporation of Ga_2O_3 at the expense of CaO in the composition of SNb_3Ga_3 decreased the ionicity of the chemical bonds. The study of pH variation revealed that the presence of Ga decreases the solubility of the glass influenced by a reduction in non-bridging oxygens (NBOs) concentration, which in turn is associated with an increase in glass network connectivity.

Keywords: Bioactive glass, ion therapy, niobium, gallium, biomaterials.

1. Introduction

Osteosarcoma accounts for a large number of deaths worldwide with an average 5-year survival rate is 60%, and children and teenagers are the groups most affected by this type of cancer[1, 2]. Recurrence is another issue with this type of cancer, as patients may develop another osteosarcoma or even lung cancer shortly after the first bone tumor [3, 4]. The most common treatment is the surgical removal of the affected area followed by systemic chemotherapy, allowing micro-metastatic control, and playing an important role in healing[1, 5]. Currently, the mechanisms used, *e.g.*, small molecules that affect the tumor-signaling pathway and immunotherapy[5, 6], do not adopt a multifunctional approach because they do not aim for the recovery of the patient's life quality through bone regeneration. This issue would be very interesting due to the surgical removal of part of the bone tissue[6, 7].

To address these problems, an interesting alternative is the use of bioceramics[8-10] such as bioactive glasses (BG) for targeted ionic therapy[11, 12], through the release of ions that, at the same time, enhance osteogenic response and control micrometastasis. BGs are recognized as bone repairing agents[13-15], with the ability to establish a stable chemical bond with the host tissue and induce cellular responses through the control and direct activation of genes associated with osteogenesis. Moreover, they can be used as platforms for drug delivery systems in diverse therapeutic fields, such as cancer, bone tissue engineering therapies, and anti-infective treatments [16, 17].

Several compositions of BG have been investigated, and the niobium (Nb) bioactive glasses occupy an important position due to the positive effect of such an element on bone healing[18, 19]. The structural role of Nb^{+5} in the silicate glass network tends to assume the octahedral coordination geometry towards oxygen (NbO_6) in glasses[20, 21]. As a result, the

presence of Nb octahedrons distorts the backbone of the glass set up by silicon tetrahedra (SiO_4) by the forming $[\text{SiO}_4]-[\text{NbO}_6]-[\text{SiO}_4]$ polyhedron structures and, hence influencing the glassy reactivity[18]. The controlled release of Nb species has been associated with improved bone regeneration by promoting alkaline phosphatase, essential for bone growth[22]. Moreover, the incorporation of small amounts of Nb_2O_5 (less than 5% mol) in the composition of the 45S5 bioactive glass has promoted an increase in biocompatibility and bioactivity of the proposed ceramic material[19-21]. Previous results conducted with niobium-containing glasses (BGNb) revealed that BGNb glasses were nontoxic to BMMSCs, instead, they stimulated greater cell proliferation, and their dissolution products are osteogenic as they differentiated BM-derived cells towards osteoblast lineage[23, 24]. *In vivo* experiments showed that BGNb were osteoconductive, enabling the formation of a bone layer onto its surface and stimulating the osteogenic cells of the periosteum to form bone[23].

Another important composition, glass-containing gallium (Ga) has been explored as an alternative for the treatment of bone cancer due to the selective antitumor action of the Ga^{+3} in the affected cells[11, 25]. The key element that characterizes the specificity of Ga^{+3} to kill cancer cells appears to be the difference in the number of transferrin receptors (TfRs) in the cell membranes of osteosarcoma cell lines (Saos2) and normal human osteoblasts (NHOsts)[12, 25]. Due to their high proliferative activity, cancer cells have more TfRs than healthy cells, which allows them to internalize large amounts of Fe^{3+} , an ion essential for DNA synthesis and cell division. This fact proves to be an advantage for therapy with Ga, as Ga mimics Fe, binds to the transferrin ligand, and is internalized in cells via a TfR-dependent pathway[12]. Upon reaching a certain threshold, the high intracellular concentration of gallium is toxic to the cell, inducing programmed cell death by the intrinsic pathway by disrupting the mechanisms of DNA synthesis and triggering caspase-

dependent apoptotic processes. In this sense, controlled release of Ga^{+3} from the vitreous matrix at critical concentration may present effective anticancer activity through ion therapy[26, 27]. Another advantage of the Ga ion is its ability to track osteosarcoma cells due to the high similarity between Ga^{+3} and Fe^{+3} , which tends to accumulate in the tumor region (even when the Ga^{+3} ions are not released close to the tumor)[28]. In addition, Ga^{+3} ions exhibit great antibacterial activity, which is interesting to prevent infections after surgery[29]. Once released into the physiological environment, Ga^{3+} can disrupt the Fe^{3+} metabolism of many infecting microorganisms unable to differentiate between the two trivalent cations. The substitution of Fe^{3+} , an active redox species essential in electron transport and oxidative stress, by Ga^{3+} , an inactive redox is the mechanism that explains the elimination of these microorganisms[30]. The structural role of Ga^{3+} in the network of a phosphosilicate glass appears to play an intermediate role due to the ability of this ion to assume tetrahedral and octahedral coordination geometries toward oxygen [12, 30].

The design of BG that combine the above-mentioned ions would match optimally the ability of Nb to accelerate bone repair while releasing essential Ga ion for antibacterial and anticancer activity. However, the synthesis of the resultant material is not trivial, especially because complex compositions tend to separate phases and not form glass. Herein, we report the synthesis and characterization of multicomponent bioactive glasses derived from the $\text{SiO}_2\text{-CaO-P}_2\text{O}_5\text{-Nb}_2\text{O}_5\text{-Ga}_2\text{O}_3$ system prepared by an innovative process based on the citric acid-assisted sol-gel synthesis coupled to the self-propagating combustion [31, 32]. To the best of our knowledge, this is the first time that multicomponent glasses, with high structural homogeneity, containing gallium and niobium have been prepared and studied for a biomedical purpose. Although the synthesis of bioactive glasses containing Nb or Ga by the sol-gel method has been reported in the literature[33, 34], these studies describe the formation of glass-ceramics or even do not provide an

adequate characterization of the prepared material, which does not allow inferences about the formation of glass properly.

2. Materials and Methods

2.1. Synthesis of bioactive glass samples

All glass compositions were prepared using the sol-gel synthesis route assisted by molecular templates and coupled to the self-propagating combustion method[31, 32, 35]. Two new glass compositions of the bioactive glasses, such as SNb3 (60% SiO₂, 36% CaO, 1% P₂O₅, and 3% Nb₂O₅ in mol%) and SNb3Ga (60% SiO₂, 33% CaO, 3% Ga₂O₃, 1% P₂O₅, and 3% Nb₂O₅ in mol%) were explored. SNb3 bioactive glass was synthesized by combining the so-called glass network-former solution (GNFS) and glass network-modifier solution (GNMS)[31, 32]. The GNFS sol was prepared by acid-catalyzed hydrolysis of TEOS and TEP, which was maintained for 12 hours under vigorous stirring at 25°C. A third solution containing species of niobium stabilized was incorporated into the GNFS solution and kept under stirring for 2 hours, resulting in a sol called GNFSNb. The GNMS solution is the source of the species that will act by modifying the vitreous network by breaking the Si-O-Si bonds. In this case, GNMS solution for SNb3 composition is composed of calcium ions (Ca(NO₃)₂·4H₂O), which were added slowly to the GNFSNb solution and stirred for 4 hours to result in a transparent solution giving rise to sol, which rapidly evolves toward the gel. A similar procedure was employed for the SNb3Ga3, except for the presence of gallium ions in the glass network-modifier solution (GNMSGa). The precursor gel of each bioactive glass was aged for 12 hours at room temperature and then dried in a vacuum desiccant cabinet at 25°C to obtain the xerogel.

2.2. Optimization of the calcination temperature

The optimal calcination temperature was investigated considering the thermal and microstructural aspects. Simultaneous measurements of Thermogravimetry and Differential Thermal analysis of the xerogel (5 mg of the sample) were performed in an analyzer (model DTG60) (Shimadzu Corporation, New Castle, DE, USA). Analysis was performed under an airflow rate of 50 mL min⁻¹ in the temperature range of 30 to 1000°C at a constant heating rate of 10°C·min⁻¹. The effect of calcination temperature on the structure was investigated by X-ray diffraction (XRD), which was collected using a diffractometer (XRD-7000, Shimadzu Scientific Instruments, Tokyo, Japan) with a Bragg Brentano camera geometry, Cu-K incident radiation ($\lambda = 1.5418 \text{ \AA}$), 40 kV, 30 mA, and acquisition rate of 2° min⁻¹ within the range 10 to 60° (2 θ). The short-range structure of xerogels was analyzed by Fourier Transform Infrared spectroscopy (FTIR) by an interferometric spectrometer (Shimadzu Prestige-21, Shimadzu Corporation, Tokyo, Japan). KBr pellets were prepared by mixing 1 mg of the sample with 100 mg of potassium bromide. FTIR spectra were acquired in the region 1800-400 cm⁻¹ with a spectral resolution of 4 cm⁻¹ and 64 scans. The xerogel was calcined at a constant heating rate of 5 °C·min⁻¹ in the temperature range of 200 to 900°C with isothermal of 10 minutes for 200, 300, 400, 500, 600, 700, 800, and 900°C.

2.3. Characterization of bioactive glass samples

The glass particle's morphology and elemental composition of glass samples were investigated by scanning electron microscopy (Thermo Fisher Scientific Inspect F50, Thermo Fisher Scientific, Hillsboro, Oregon, USA) with an energy-dispersive X-ray spectroscopy (EDS) analyzer (NORAN™ System 7 X-ray Microanalysis System, Thermo Fisher Scientific, Inc., Waltham, MA, USA).

A surface area and porosimetry analyzer (Micromeritics ASAP 2020) was used to measure the Brunauer-Emmett-Teller (BET) surface area and pore size distribution. The residual water inside samples was removed via pre-heating at a high temperature (200 °C). Samples were assessed at liquid nitrogen temperature after being gassed at 200 °C under the flow of N₂ for 2 h.

The glass microstructure was investigated by Raman spectroscopy by using a triple spectrometer Raman system (T-64000, HORIBA Jobin Yvon S.A.S., Longjumeau, France) equipped with a detection system Charge Couple Device (CCD). Collection of the scattered light in the backscattering geometry was made using a confocal microscope (BX41, Olympus optical CO. LTD, Tokyo, Japan) with a 150x objective to collect the Raman signal, which in turn was spectrally analyzed with a spectrometer with a typical resolution of 2 cm⁻¹. Raman spectra were recorded between 200 and 1300 cm⁻¹, using the 532 nm exciting lines. The power of illumination was 10 mW.

2.4. Physical properties investigation

Bulk density (ρ_{Bulk}) is defined as the mass of a unit volume of dry sediment, including both solids and pores. The bulk density for the samples of the bioactive glasses was measured using a powder densimeter (Powdermix[®] LTDA). All measurements were performed in triplicate and the standard deviation of the means was calculated. Obtained density values were used to calculate the molar volume using the relation $V_m = \sum_i x_i M_i / \rho_{Bulk}$, where x_i is the molar fraction and M_i is the molecular weight of the i th component M . The molar volume of oxygen (V_O) is the volume of glass in which 1 mole of oxygen is contained. These values were calculated using the relation $V_O = V_m / \sum_i x_i M_i$. Oxygen packing density (OPD) was calculated using the relation $OPD = \sum_i x_i n_i / V_m$, where x_i is the molar fraction of an oxide R_mO_n and n_i is the number of

oxygen atoms of this oxide. The ionic character or bond ionicity (I_B) can be used to describe the nature of chemical bonding in glass based on the following parameters: electronegativity difference of the glass constituent oxide ($\Delta\chi = \chi_A - \chi_C$, where χ_A and χ_C are the Pauling electronegativity of the anion (oxygen) and that of the cation) and Pauling's ionicity ($I_B = 1 - \exp(-0.25\chi(\Delta\chi)^2)$)[36].

2.5. pH and Zeta potential measurements of glassy dissolution

The solubility of the glassy matrix can be indirectly investigated through pH variations as a function of soaking time using automatic titration equipment Particle Metrix (Stabino, GmbH). Variations in zeta potential were monitored in the same experiment concomitantly with pH measurements. For suspensions of the bioactive glass particles in deionized water, the zeta potential is the electrical potential difference between the dispersion medium and the stationary layer of fluid attached to the dispersed particle.[37] The experiment measured and recorded the pH and Zeta values every 7.5s for 24 hrs. Toward this purpose, 10 mg of the glass particles were soaked in a beaker with 10 mL of deionized water with an initial pH value set at 7.4 for all experiments [38]. The zeta potential, ZP (mV) was calculated using the relation $P_{IP} = kv_0\varepsilon ZP/\eta$. Where P_{IP} is the particle interface potential, k is the instrument constant, v_0 is the maximum velocity of the liquid, ε is the dielectric constant, and η viscosity of the liquid.

3. Results and Discussion

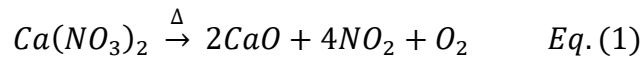
3.1. Obtaining SNb3 and SNb3Ga3 xerogels

The glass network-former solution containing niobium species was transparent without any presence of visible inhomogeneities within the sol. Similarly, the glass network-modifier solutions,

i.e., GNMS and GNMSGa, displayed a clear and colorless solution. The resulting sol formed by glass network-former solution and glass network-modifier solution showed a continuous increase of viscosity of the medium rapidly toward the gel, preserving its optical characteristics without the presence of apparent precipitates. The xerogels were obtained by spontaneous drying of the gels inside vacuum desiccant cabinets and the air was continuously evacuated which allowed the removal of solvents and ensured the homogeneity of the glass precursor matrix[32].

The ideal calcination temperature was initially investigated by the thermal stability of xerogels through TGA and DTA analyzes (**Figure 1a-b**). The TGA curves for the SNb3 and SN3Ga3 xerogels revealed a similar profile, exhibiting the same total mass loss of 67 % related to different thermal events. The large loss of mass observed for both xerogels was due to the high organic load conferred by the presence of molecular template present in the citric acid-assisted sol-gel route coupled to the self-propagating combustion method[31, 32, 35]. By analyzing the details present in the TGA curves, it was possible to notice that the SNb3 and SN3Ga3 xerogels exhibited an initial mass loss of 5% in the region of 50-120°C, attributed to the loss of residual solvent molecules from synthesis and by-product of the hydrolysis of TEOS and TEP[32, 35, 39]. The second thermal event was comprised of a wide temperature range (150-250°C): two exothermic peaks around 173°C and 178.0°C associated with a weight loss of 41% for both glasses, which can be attributed to the oxidation of the organic charge catalyzed by the nitrate ions, *i.e.*, self-propagating combustion[32]. A third mass loss of 18% in the region of 310-420°C was related to the superposition of at least three exothermic events: (i) removal of the residual organic product from the precursors' decomposition, (ii) condensation of vicinal OH groups, and (iii) geminal OH groups present on the xerogel surface[32, 39].

The structure of the xerogels was monitored during the calcination stage for SNb3 and SN3Ga3 samples by X-ray diffraction (**Figure 1d-e**). The diffractograms for SNb3 as a function of the thermal treatment temperature showed an amorphous structure for the sample calcined at 200°C, which still preserved the structural characteristic of the dehydrated xerogel. Xerogels calcined at temperatures above 300°C exhibited a small peak at $2\theta = 25^\circ$ attributed to the presence of residual nitrate species from the thermal event associated with self-propagated combustion[31, 32]. The presence of NO_3^- species trapped within the pores of the xerogel remained thermally stable above 500°C, decomposing upon heating up to 600°C to release nitrogen dioxide, **Eq. (1)**[32].



The diffractogram of SNb3 xerogel calcined at 600°C revealed a non-crystalline structure typical of glassy materials and corroborates thermal data. Similar results can be observed for xerogel calcined at 700 or 800°C, which was also characterized by a structural disorder. On the other hand, it was possible to observe the presence of the following diffraction peaks: $2\theta = 21.87, 23.15, 25.36, 26.83, 28.93, 29.95, 36.23, 38.17, 41.19,$ and 49.95° for the SNb3 xerogel calcined at 900 °C. This XRD pattern is consistent with the formation of β - wollastonite - β -CaSiO₃ (JCPDS 290372) and calcium meta niobate - CaNb₂O₆ (JCPDS 391392) crystal phases²⁶. No diffraction peaks were observed for SNb3Ga3 xerogel calcined up to 600°C, indicating that the self-propagated combustion process was more efficient in the removal of nitrate species in the matrix. Findings from an in-depth analysis of the diffractogram showed subtle imperfections in the diffractogram in the region of $2\theta = 23$ - 28° arising for xerogel calcined from 700°C, reaching thus a complete devitrification at 900°C. β - wollastonite (JCPDS 290372) and calcium meta niobate of gallium was observed in the diffraction pattern.

INSERT FIGURE 1

Figure 1. Investigation of the thermal behavior of SNb3 and SNb3Ga3 xerogels: (a) thermogravimetric analysis curves (TGA), (b) derivative thermogravimetric analysis curves (DTG), and (c) differential thermal analysis (DTA) curves. Studies on structural evolution by X-ray diffraction of the xerogels calcinated at various temperatures: 200, 300, 400, 500, 600, 700, 800, and 900°C. Data collection by X-ray diffraction was performed after the samples were heated at a rate of 10 °C·min⁻¹ to the target temperature followed by a 10-minutes isotherm.

Based on thermal results the minimum temperature required for the calcination of the xerogels would be about 600°C[32]. The evolution of the short-range order (SRO) and long-range order (LRO) as a function of calcination temperature within the atomic structure of the xerogels step was carried out by FTIR (**Figure 2**). The FTIR spectrum over the range 4000-370 cm⁻¹ was dominated by the vibrations of the following chemical bonds: Si-BO, Si-NBO, -O-H, Nb-O, and C-O.[40, 41] In the high-frequency region, it was possible to observe continuous dehydration and loss of hydroxyl groups from the xerogel characterized by the decreasing absorption band attributed to the O-H stretching, as the calcination temperature was increased (**Figures 2a_i** and **2b_i**). Furthermore, it was possible to note the disappearance of absorptions in the 2850-2975 cm⁻¹ region associated with the C-H stretch present in the -CH₂- and -CH₃ groups for xerogels calcined above 300°C.[32] At intermediate frequencies were located the vibrational modes of the carbonyl in the carboxylate group (1700-1750 cm⁻¹), carbonates species (1350-1700 cm⁻¹), deformation mode of undissociated water molecules ($\delta_{\text{H-O-H}}$) at 1640 cm⁻¹, and nitrate species ($\nu_3(D_{3h}) = 1385$ cm⁻¹) (**Figures 2a_{ii}** and **2b_{ii}**).[38] The FTIR data showed that most of the nitrate species were consumed in the oxidation of the organic load of the xerogel matrix up to 300°C for SNb3 and SNb3Ga3 (self-propagating combustion method)[31, 32].

The region of lower frequencies was characterized by the presence of the structural band (SB; 1000-1280 cm⁻¹), which allows obtaining photographs of some steps present in the structural transformations of xerogel important in the formation of the vitreous network (**Figures 2a_{iii}** and

2b_{iii}). A similar trend can be noted for SNb3 and SNb3Ga3 xerogels as a function of calcination temperature. Initially, dried xerogels at 60°C exhibited a silicate matrix predominantly formed by highly crosslinked structures (Si-BO-Si, $_{\text{Si}}\text{Q}^3$ or $_{\text{Si}}\text{Q}^4$), which progressively breaks down to form Si-NBO with increasing calcination temperature, *i.e.*, entry of network-modifying ions (Ca^{2+}) in the silicate network ($\text{Si-O-Si} \rightarrow \text{Si-O}^- \text{Ca}^{2+} \text{O-Si}$). A detailed analysis of the maximum absorption for the SB revealed that it reached a frequency of 1040 cm^{-1} (minimum value) and the highest value of full width at half maximum (FWHM) for the xerogel calcinated at 600°C, indicating the consolidation of the glass network[32, 40]. The frequency of SB increased again towards the higher energy for xerogels calcined at temperatures above 700°C, indicating changes in short-range ordering in the glassy microstructure[42, 43]. These changes preceded the devitrification observed in xerogels calcined at 900°C and the formation of β -wollastonite characterized by the vibrational frequency of the structural band around 1100 cm^{-1} [42, 44]. The presence of the calcium meta niobate was confirmed by absorptions at 497, 550, 750, 810, and 870 cm^{-1} (represented by the symbol \clubsuit in the spectra) for both xerogels[45].

INSERT FIGURE 2

Figure 2. Structural evolution as a function of calcination temperature is monitored by infrared spectroscopy (FTIR) for (a) SNb3 and (b) SNb3Ga3 xerogels. Data collection by FTIR was performed after the heat at a rate of $10 \text{ }^\circ\text{C}\cdot\text{min}^{-1}$ to the target temperature followed by a 10-minutes isotherm.

Based on data obtained by thermal analysis, X-ray diffraction, and infrared spectroscopy, the calcination temperature of xerogels was optimized at 600°C for 24 hours to obtain SNb3 and SNb3Ga3 bioactive glass.

3.2. Chemical and microstructural characterization of bioactive glasses

X-ray diffraction pattern for the annealed glass samples reveals the presence of broad signals characterized by diffuse rings that are typical of materials in which translational periodicity

is absent. (**Figure 3a**). The diffractogram for 58S glass reveals the presence of a large amorphous halo in the region of $2\theta = 12-37^\circ$, while for the BGNb glasses it is possible to observe two broad peaks. The first band at $2\theta = 11.3^\circ$ was associated with the leakage of the incident X-ray beam due to scattering by the sample chamber and/or dust. The second peak for BGNb glasses exhibits slightly different maxima, i.e., $2\theta = 30.2^\circ$ for SNb3 and $2\theta = 29.9^\circ$ for SNb3Ga3. In addition, the diffractogram profile for SNb3Ga3 glass presents a wide asymmetric halo exhibiting a tail towards lower 2θ values. It is noteworthy that the presence of the halo extending to smaller 2θ for SNb3 glassy materials means a longer distance from any central atom, i.e., fewer atoms in the secondly nearest neighbor, which implies a slightly lower density for SNb3Ga3 compared to SNb3 glass, in consistent with the densities measured for BGNb glasses (*Table 1*). This result suggests for the SNb3 glass the existence of a greater amount of modifier ions, in the case of Ca^{2+} , inside the empty polyhedra of the loose silicate network[46].

INSERT FIGURE 3

Figure 3. (a) XRD patterns of 58S, SNb3, and SNb3Ga3 bioactive glass glasses, showing the typical amorphous halo. Investigations of the short-range ordering of glasses by vibrational spectroscopies: (b) FTIR spectra and (c) Raman spectra of SNb3 and SNb3Ga3. Data relating to 58S bioactive glass has been added for comparison purposes and to support discussions.

FTIR results for the annealed glasses corroborated the XRD data, confirming the glassy nature of the samples (**Figure 3b**). The structure of silicate glasses in a wide compositional range has been studied using Raman and FTIR spectroscopy.[21, 47, 48] In short, infrared spectra showed the dominance of the main vibrational modes present in 58S bioactive glass: (i) the absorption at 1040 cm^{-1} can be assigned to Si-O stretching modes associated with mainly SiO_4 tetrahedra involving bridging oxygens; (ii) the band at 1200 cm^{-1} can be associated with polymerized SiO units; (iii) the low-intensity signal at 785 can be attributed to the Si-O stretching modes that involve bridging oxygens (Si-BO-Si); (iv) at 460 cm^{-1} related to O-Si-O bending

modes; (v) while the shoulder at 940 cm^{-1} toward lower-frequencies can be related with Si-O stretching modes involving non-bridging oxygens (Si-NBO).[49] In the present case, the infrared absorption related to NbO_6 octahedra occupying a position equivalent to that of SiO_4 tetrahedra, linking the separate Si-O groups in the glassy network, cannot be visualized in the infrared spectrum due to the low Nb content in the glassy composition and the proximity of the absorption frequency of the Si-O-Nb and Si-BO-Si groups.

A detailed analysis of the FTIR spectra revealed a red shift in the frequency of the maximum of the structural band (SB) ranging from 1045 cm^{-1} for 58S, evolving to 1040 cm^{-1} for SNb3 glass, and reaching a frequency of 1036 cm^{-1} for SNb3Ga3 bioactive glasses (**Figure 3c**). In our previous paper[21], we investigated the role played by niobium in the structure of alkali-containing alkaline-earth niobophosphosilicate glasses prepared by the melt-quenching technique. Our findings indicate that the structure of such glasses is formed by SiO_4 tetrahedra and distorted NbO_6 octahedra, in which each octahedron shares its corners with SiO_4 tetrahedra forming a common network with strong Si-O-Nb bonds.[21, 41] In addition, the NbO_6 octahedra can cross-link several oxygen sites, breaking Si-O-Si bonds to form various polyhedral $[\text{Nb}(\text{OM})_{6-y}(\text{OSi})_y]$, where $1 \leq y \leq 5$ and M = network modifying ions or P forming Nb-O-P bonds in the terminal sites[21]. Similar structural behavior for niobium in the silicate network would be expected for the sol-gel glasses investigated here.

Ga_2O_3 is known as intermediate glass forming oxide, which can act either as a modifier with Ga^{3+} in sixfold coordination or as glass former with Ga^{3+} in fourfold coordination, depending on alkali content. Gómez-Cerezo *et al.*[50] reported a detailed structural study for bioactive glasses derived from the $\text{SiO}_2\text{-CaO-P}_2\text{O}_5\text{-Ga}_2\text{O}_3$ system, in which the local environment of Ga^{3+} has been characterized using ^{29}Si , ^{71}Ga , and ^{31}P MAS NMR analysis, demonstrating that Ga^{3+} is efficiently

incorporated as both, network former (GaO_4 units, about 70%) and network modifier (GaO_6 units, about 30%). Although Ga plays an intermediate structural role in several glass compositions, in the case of the bioactive glass SNb_3Ga_3 , it seems to have a marked network former role. In other words, the entry of Ga^{3+} into the vitreous network promotes an increase in the network connectivity, contributing to an increase in the degree of polymerization of the glass, since part of the calcium ions that behave as network modifying agents were replaced by gallium ions that act as network formers, and hence a replacement of part of the $\text{Si-O}\cdots\text{Ca}^{2+}\cdots\text{O-Si}$ by Si-O-Ga-O-Si bonds[30]. In fact, the total network connectivity which accounts for all network former (Si and P), intermediate ions (Nb and Ga), and modifier and/or charge compensator cations increases from 2.9 for SNb_3 to 3.0 for SbNb_3Ga_3 (**Table 1**).

The frequency of the structural band is influenced by several factors such as bond length and angles, electronegativity, and atomic mass of the elements present in the vicinity of the silicon tetrahedrons that make up the backbone of the glass. In general, the frequency of the SB band tends to shift to lower energies as the size of the Si-O chemical bond increases and, consequently, becomes weaker. The mean Si-O distance is in the range of 1.58-1.60 Å independently on the glass composition, whereas the Nb-O bond distance can range from 1.6 to 2.4 Å[30, 51]. Higby *et al.*[52] studied several compositions of alkali galliosilicate glass and observed that the average Ga-O bond distance with predominant tetrahedral coordination was 1.83 ± 0.01 Å, independent of glassy composition. On the other hand, the mean Ga-O bond distances for the $\beta\text{-Ga}_2\text{O}_3$ system, where Ga ions were presented both in tetrahedral and octahedral sites, were 1.821 and 2.013 Å, respectively[52, 53]. The presence of niobium octahedra [NbO_6] and gallium polyhedra [GaO_x] in the silicate network can promote changes in the lengths and angles of the Si-O bonds, in order to accommodate the Nb and Ga polyhedra and minimize the structural distortions of the vitreous

matrix. It is noteworthy that the frequency of the vibration is inversely proportional to the reduced mass and directly proportional to the force constant. Recognizing that niobium and gallium are less electronegative ($\chi^{\text{Nb}} = 1.6$ and $\chi^{\text{Ga}} = 1.6$) and heavier ($m^{\text{Nb}} = 92.9064\text{u}$ and $m^{\text{Ga}} = 69.723\text{u}$) elements than silicon ($\chi^{\text{Si}} = 1.8$, $m^{\text{Si}} = 28.0855\text{u}$), a redshift to infrared absorption frequency would be expected for Si-O-Ga bond in comparison with Si-O-Si bond[21]. In fact, it is possible to observe a slight widening of the SB with a slight asymmetry toward lower frequencies is notable, slightly decreasing the separation between the absorptions related to the symmetric stretching mode of the SiO_4 groups (785 cm^{-1}) and the absorption band onset at 825 cm^{-1} associated with the stretching modes of the Si-O bond. Additionally, the phosphorus environment for SNb3 and SNb3Ga3 glasses exists as an orthophosphate complex $[\text{PO}_4]^{3-}$ ($500\text{-}600\text{ cm}^{-1}$), rather than entering the silicate glass network[13, 31, 32].

Raman spectroscopy was employed to gain more information on the glass microstructure (**Figure 3d**). Such a technique is very powerful to investigate the chemical environment of heavy elements (*i.e.*, Nb and Ga) within a glass matrix due to its larger polarizability and hence high scattering cross-section, which overshadow the signal related to the Si-O vibrational modes. No absorption related to Nb-O-Nb species was observed in the vibrational spectra of the glasses ($\sim 570\text{ cm}^{-1}$). The absence of the Nb-O-Nb species is important from the point of view of bioactivity since the presence of these chemical bonds has been associated with the bioinactivation of glassy compositions[20, 21, 23, 24]. Raman spectrum for SNb3Ga3 glass showed absorption in the range of $640\text{-}720\text{ cm}^{-1}$ associated with the bending and stretching of GaO_4 units in the glass network[54]. The presence of small absorptions at 365 , 511 , and 550 cm^{-1} were attributed to the symmetric stretching and bending vibrations of GaO_6 octahedra[54, 55]. The occurrence of NbO_6 octahedra bonded with SiO_4 tetrahedra in the O-Si-O-Nb-O-Si-O units was manifested by the strongest

absorption at 820 cm^{-1} for SNb3 and 810 cm^{-1} for SNb3Ga3 glass[21, 56]. This result suggests the NbO_6 octahedra are less distorted for SNb3Ga3, probably due to the presence of GaO_x groups with different coordination numbers, which can assume configurations that minimize the distortion of the niobium polyhedral. Such results would be indicative of a preferential association of gallium, especially those in an octahedral site, with niobium octahedra in the vitreous network.

The frequency of symmetric stretching of SiQ^2 species and symmetric stretching of PO_4^{3-} group moved from 956 cm^{-1} for 58S, evolving to 950 cm^{-1} for SNb3 glass, and reaching a frequency of 944 cm^{-1} for SNb3Ga3 bioactive glasses[40]. This redshift is related to the presence of NbO_6 and GaO_x polyhedra in the glassy network (Si-O-Si), affecting the chemical environment of Si and the vibration of the Si-O bond in SiQ^2 species. The absorption at 1080 cm^{-1} for SNb3 and at 1088 cm^{-1} for SNb3Ga3 was related to the overlapping of asymmetric stretching of bridging oxygen in all SiQ^3 species and the shortest Nb-O bond present in the NbO_6 octahedra - niobyl group (Nb=O)[41]. This blueshift is associated with an increase in Nb-O bond order and/or a shortening of the Nb-O bonds in the NbO_6 octahedra induced by the presence of GaO_x polyhedra in the vicinity[51].

The morphology of the glass samples was investigated by using SEM microscopy, whereas the chemical composition was determined by using energy-dispersive X-ray spectroscopy (**Figure 4a-h**). SEM microscopy for SNb3 and SNb3Ga3 annealed glass samples revealed a morphology and porosity structure characteristic of mesoporous bioactive glass (MBG). SEM observation also indicated that both samples were mesoporous and formed by the stacking of nanometric plates, generating material with a high surface area and high porosity. These features are critical factors for the control of glass reactivity and bioactivity, which are very important for biomedical applications³⁵. The EDS analysis confirmed the presence of the Si, O, Nb, Ca, and P for SNb3

glass and chemical composition similar to the nominal (**Figure 4d and 4h**). In addition to these species, the presence of Ga was determined for SNb3Ga3 glass, and the proposed glass chemical composition modification was confirmed by EDS quantification (**Figure 4g and 4h**).

INSERT FIGURE 4

Figure 4. Morphology and chemical composition of glass samples obtained by SEM-EDS analysis. Data for SNb3 glass: SEM images showing (a) the morphology of the glass and (b) the region analyzed by the EDS probe, (c) the EDS spectrum collected, and (d) the molar composition table confirming the chemical composition of SNb3 glass. Data for SNb3Ga3 glass: SEM images showing (e) the morphology of the glass and (f) the region analyzed by the EDS probe, (g) the EDS spectrum collected, and (h) the molar composition table confirming the chemical composition of SNb3Ga3 glass.

To obtain a deeper knowledge of the mesoporous structure, textural properties were analyzed by the N₂ adsorption/desorption method. The N₂ adsorption-desorption isotherm of SNb3 and SNb3Ga3 annealed glass was almost ideally type-IV isotherm as defined by IUPAC, which is a characteristic isotherm for mesoporous materials (**Figure 5**)[57]. The surface area and pore volume of the SNb3Ga3 sample were 37.2% and 56.3% smaller, respectively than those observed for SNb3 glass (see **Table Inset in Figure 5**). Gómez-Cerezo *et al.*[50] also reported a drastic decrease in surface area and pore volume after Ga incorporation into two distinct bioactive glasses (58S and 85S) derived from the SiO₂-CaO-P₂O₅ system. The shrinking of pore volume and surface area was due to a non-retention of the pore architecture copied from the precursor xerogel microstructure during the calcination step to the organic load removal. The self-propagating combustion step promotes spot heating in the glass, which can result in pore blockage and macropore collapse (affecting adsorption capacity and diffusion rates)[57]. The pore size distributions of the isotherm adsorption branch showed a heterogeneous pore size distribution, which displayed a wide pore size distribution centered at 105 Å for SNb3 and 79.1 Å for SNb3Ga3. These porous characteristics presented by glasses are very important for the chemical and

biological processes that culminate in the integration of the material with living tissue, and they are attractive for a variety of biomedical applications, including drug delivery[58-61].

INSERT FIGURE 5

Figure 5. N₂ adsorption-desorption isotherm of SNb3 and SNb3Ga3 annealed glass: type-IV isotherm as defined by IUPAC.

3.3. Physical properties investigation

The network connectivity number is important to understand the material's dissolution behavior, since the hydrolysis of silicate species with an average number of bridging-oxygen (BO, Si-O-Si type species) greater than three requires high-cost energy, increasing the time needed to start the reactions that culminate in biomineralization. The theoretical network connectivity (NC) for both SNb3 and SNb3Ga3 bioactive glass was calculated as described by Hill *et al.*[62]. The calculation of network connectivity of glass is based on the relative number of network-forming oxide species and network modifying species present (**Table 1**).

Table 1. Network connectivity (NC), bulk density (ρ_{Bulk}), molar volume (V_m), oxygen molar volume (V_o), oxygen packing density (OPD), and ionicity (I_B) of SNb3 and SNb3Ga3 bioactive glass.

Glass	NC	ρ_{Bulk} ($g \cdot cm^{-3}$)	V_m ($cm^3 \cdot mol^{-1}$)	V_o ($cm^3 \cdot mol^{-1}$)	OPD ($mol \cdot L^{-1}$)	I_B
SNb3	2.91	0.819	80.10	45.51	21.97	0.5829
SNb3Ga3	2.98	0.748	93.06	51.13	19.56	0.5733

NC values were calculated for SNb3 and SNb3Ga3 compositions assuming that all phosphorus species occupy tetrahedral sites, while niobium species occupy octahedral sites. For the Ga species, it was assumed that 60% of the Ga species are in tetrahedral sites and the remaining 40% are in the octahedral form for the SNb3Ga3 glass[50]. All Nb and 60% of Ga species are participating in the vitreous network through the bonding between the Nb and Ga polyhedra with the silica tetrahedra, SiO₄. The molar volume (V_m), oxygen molar volume (V_o), oxygen packing density (OPD), and ionicity (I_B) for SNb3 and SNb3Ga3 bioactive glass were calculated using the relations described by Moustafa *et al.*[36]

The data obtained showed that the incorporation of small molar fractions of Ga₂O₃ at the expense of CaO content resulted in increased network connectivity for SNb3Ga3 glasses by the incorporation of Ga ions into the silicate network. Furthermore, the incorporation of Ga₂O₃ at the expense of CaO in the composition of SNb3Ga3 resulted in an 8.7% reduction in the measured

density value and consequently promoted a 16.2% increase in the calculated molar volume compared to gallium-free glass (SNb3). The density of the glasses increases with increasing the concentration of modifier and/or charge compensator cations, as well as with the atomic number/mass of the particular modifier cation present[63].

In the present case, density was primarily influenced by a reduction in NBOs concentration, which in turn is associated with an increase in glass network connectivity. It is worth highlighting that each NBO must be associated with a nearby modifier cation (Ca^{2+}) to maintain local charge neutrality. These modifier cations occupy the interstices in the network, reducing the unoccupied free volume of the structure, and contributing to the density increase. The incorporation of Ga_2O_3 at the expense of CaO in the composition of SNb3Ga3 resulted in a decrease in the concentration of NBOs and, consequently, an increase in the concentration of bridge oxygen, proportionally to the number of modifier cations reduced in the composition. Consequently, it led to the formation of a less compact network associated with the increase of V_m and a decrease in density. This structural effect seems to overcome the increase in the greater atomic mass of Ga_2O_3 .

The determined oxygen molar density and oxygen packing density (*OPD*) of SNb3 and SNb3Ga3 samples showed an increase in V_o from 45.51 to 51.13 $\text{cm}^3 \cdot \text{mol}^{-1}$, respectively, which was associated with a decrease in oxygen packing density from 21.97 to 19.56 $\text{mol} \cdot \text{L}^{-1}$ (**Table 1**). Such results confirm an increase in bridging oxygen bond density associated with a decrease in the number of bonds per unit volume of the glass due to the expansion of the glassy network. Furthermore, the incorporation of Ga_2O_3 at the expense of CaO in the composition of SNb3Ga3 decreased the ionicity of the chemical bonds (**Table 1**). The covalent bonding would be a consequence of the polycondensation of $[\text{GaO}_4]$ tetrahedra with the $[\text{SiO}_4]$ tetrahedrons, favored

in the acid-catalyzed sol-gel synthesis. In fact, FTIR and Raman spectra showed an increase in the covalent character of the chemical bonds in SNb3Ga3 glass by the decrease of ionicity.

3.4. Glass dissolution studies

According to the Hensch mechanism[64], the earliest events that occur on the glass surface in the physiologic medium is the departure by ion exchange of labile ions from the glass network with H_3O^+ from solution, resulting in a decrease of acid species and then promoting a pH increase. Consequently, the exchange of protons from the aqueous medium with the ions from the glass network results in a local pH increase that accelerates the process of dissolution of the glass silicate matrix. Thus, an indirect way to study the solubility and hence the reactivity of glass in an aqueous medium is by monitoring the pH variation of the medium (**Figure 6**). Analyzing the behavior of the pH curves for the different glasses, it was possible to observe that all samples exhibit a similar set of events. (**Figure 6a**). In the initial moments, there was an abrupt increase in pH due to the intense loss of labile ions from the network, followed by stabilization, which was related to the formation of a rich layer of silica gel that passivates the vitreous surface, hindering ion diffusion and, consequently, the ion exchange.

By comparing the maximum pH values reached for each glass composition, it was possible to observe that SNb3 glasses reached a higher pH value than the SNb3Ga3 (**Figure 6b**). This trend could be associated with a reduction in the glass solubility of SNb3Ga3. The qualitative interpretation of this result is based on the correlation between solubility and NC. The lowest value of $CN=2.91$ for SNb3 indicates an open and fragmented structure, which exhibits a higher dissolution rate in the physiological aqueous medium, compared to SNb3Ga3 whose highest value of $CN=2.98$ is associated with a glass with a more interconnected network. Indeed, the ion

exchange occurs at the bioactive glass surface, in which Ga^{3+} and/or Ca^{2+} from the glass exchange with H_3O^+ from the surrounding solution. This step is controlled by the diffusion of these labile species from the vitreous network towards the solution. The Ca^{2+} - H_2O interactions are responsible for calcium ion leaching and it occurs much faster than the diffusion of trivalent species of Ga^{3+} , ~ 70% of such ions are more trapped into the glassy network[65]. The energy barrier to be overcome to break the Ga^{3+} chemical interactions within the glassy matrix, allowing its diffusion toward the solution is greater than expected for a divalent cation[65, 66]. Consequently, the presence of gallium in the glass composition does not seem to play an equally critical role in the initial dissolution stages of bioactive glasses.

The relation between soaking time and the Zeta potential (ZP, logarithmic display) is shown in **Figure 6c**. The curves for the SNb3 and SNb3Ga3 samples revealed a rapid decrease in the ZP module in the initial moments, followed by a slow and continuous decrease until reaching a stabilization level. This initial burst can be related to the release of the Ca ions from the glass network by ion exchange with H_3O^+ from the solution and the formation of anionic structures in the glass particles. The following slow decrease in the ZP modulus may be linked to the subsequent events of condensation and polymerization reactions involved in the transformation of the silica gel layer[67], while the stabilization trend observed in the curve as a function of immersion time may be related to the passivation of particles by the formation of a thin layer of apatite and/or by increasing particle size as a result of coalescence between smaller glass particles. All these effects can strongly influence the suspension stability behavior of glass particles[37]. In fact, the system containing the SNb3 glass showed good stability in the initial immersion instants with a zeta potential around -52.1 mV, reaching an incipient instability (-30.0 mV / ~pH = 10.9) after 20.7 minutes. In agreement with the pH variation data, it was possible to observe a difference in the

profiles of the Zeta potential variation curves for the SNb3 and SNb3Ga3 glasses. The suspension formed by SNb3Ga3 glass showed excellent stability (-62.0 mV) in the initial times and reached incipient instability (-30.0 mV / ~pH = 9.2) only after 4.05 hours. This difference in the stability of the glass particle suspensions is directly related to the reduction in chemical reactivity promoted by the gallium ion in the SNb3Ga3 glass matrix, manifested by the lower variation in the pH amplitude and hence a lower solubility of the silica network (pH dependent), which slows down the reactions that govern the chemical transformations that occur on the glass surface[68, 69]. Thus, the presence of Ga in the composition of SNb3Ga3 delayed the initial processes, resulting in the transformation of the glassy surface and subsequent biomineralization. It is worth pointing out that a negative ZP is interesting from the biomineralization point of view since several studies have suggested that a negative Zeta potential enhances the formation of a hydroxyapatite layer in a biological environment[70]. It is worth mentioning that the protein-surface interaction is the first event in the process of integrating an implanted device with host tissue and can determine the success or failure of the implanted device. In addition, it has been suggested that negative values of zeta potential have a significant favorable effect on the attachment and proliferation of bone cells[37].

INSERT FIGURE 6

Figure 6. (a) Studies of the pH changes as a function of soaking time in deionized water. (b) Study of the variation in pH values during the first 100s after immersion of the glass particles in deionized water. (c) The leaching behavior was also investigated through changes in the Zeta potential. (d) Proposed scheme of ions effect lixiviated from bioactive glasses on repair and regeneration and bone cancer targeted therapy.

The controlled release of Si, P, and Ca species are widely explored in the literature for bone regeneration[18-20, 71]. On the other hand, the Ga³⁺ ion is one of the most interesting therapeutic ions in the field of bone pathologies[50], whereas Nb species are recognized for their osteogenic potential[18-20]. The use of bioactive glass is strategic for this purpose because the controlled

delivery of these therapeutic ions associated with Ga^{3+} ion allows a therapy selectively targeted to bone cancer cell lines, reducing tumor cell viability [12, 25, 28], whilst still promoting normal human osteoblast cell viability and proliferation. This approach results allow us to infer that Nb- and Ga-doped ceramic biomaterial can be a powerful strategy for bone cancer targeted therapies through synergistic effects induced by ion-mediated cascade mechanism (**Figure 6d**). In this sense, the Nb and other already established ions (*e.g.*, Ca, Si) released from the proposed bioactive glass can act in osseointegration (*i.e.*, formation of hydroxyapatite, increased roughness, and *in vivo* bone repair), while cancer targeted therapies took place from Ga ion. It is noteworthy that the amount of Ga^{3+} ions delivered by the bioactive glass can be modulated through small changes in the chemical and structural composition of the bioceramic.

4. Conclusion

In sum, we propose a strategy to design bioactive glass containing niobium and gallium with high structural homogeneity where citric acid-assisted sol-gel synthesis coupled with the self-propagating combustion method were rationally used. Ga assumes both a tetrahedral and octahedral configuration, whilst niobium remains in an octahedral site with a high degree of distortion. The entry of Ga^{3+} in the glassy network contributes to the increase in the connectivity of the vitreous network, since part of the $\text{Si-O}\cdots\text{Ca}^{2+}\cdots\text{O-Si}$ bonds were replaced by Si-O-Ga-O-Si , resulting in a reduction of network modifier ions in the composition of SNb_3Ga_3 . Such results confirmed an increase in bridging oxygen bond density associated with a decrease in the number of bonds per unit volume of the glass due to the expansion of the glassy network. Furthermore, the incorporation of Ga_2O_3 at the expense of CaO in the composition of SNb_3Ga_3 decreased the ionicity of the chemical bonds.

Acknowledgments

The authors are grateful for financial support from the Coordination for the Improvement of Higher Education Personnel - CAPES (PNPD: 20131773 / Grant: 33003017034P8), the Brazilian National Council for Scientific and Technological Development - CNPq (Grant: 436164/2018-3), and São Paulo Research Foundation - FAPESP (Grant: 2010/05394-9 and 2020/00598-7). The authors thank the Plasma and Processes Laboratory (LAB-PP) of the Aeronautics Institute of Technology for FTIR and Raman analyses. This research used the facilities of the Brazilian Nanotechnology National Laboratory (LNNano), part of the Brazilian Centre for Research in Energy and Materials (CNPEM), a private non-profit organization under the supervision of the Brazilian Ministry for Science, Technology, and Innovations (MCTI). Thus, the SEM staff is acknowledged for their assistance during the experiments (SEM-C1-26147 and SEM-20210304).

Author Contributions

Medeiros GS: Methodology, Formal analysis, Writing-Original Draft. **Oliveira LFM:** Formal analysis, Writing, Review & Editing. **Ferreira FV:** Formal analysis, Writing, Review & Editing. **Souza LPL:** Formal analysis, Writing, Review & Editing. **Martin RA:** Formal analysis, Writing, Review & Editing. **Oliveira IR:** Formal analysis, Writing, Review & Editing. **Lopes JH:** Conceptualization, Methodology, Investigation, Resources, Writing - Review & Editing, Supervision, Funding acquisition.

Bibliography

- [1] M.W. Bishop, K.A. Janeway, R. Gorlick, Future directions in the treatment of osteosarcoma, *Curr Opin Pediatr*, 28 (2016) 26-33.
- [2] L.R. Sadykova, A.I. Ntekim, M. Muyangwa-Semenova, C.S. Rutland, J.N. Jeyapalan, N. Blatt, A.A. Rizvanov, Epidemiology and Risk Factors of Osteosarcoma, *Cancer Invest*, 38 (2020) 259-269.

- [3] M.S. Isakoff, S.S. Bielack, P. Meltzer, R. Gorlick, Osteosarcoma: Current Treatment and a Collaborative Pathway to Success, *J Clin Oncol*, 33 (2015) 3029-3035.
- [4] C. Eder-Czembirek, D. Moser, S. Holawe, T. Brodowicz, J. Ries, I. Sulzbacher, E. Selzer, Osteosarcoma of the jaw – experience at the Medical University Vienna and comparative study with international tumor registries, *Clinics*, 74 (2019).
- [5] D.J. Harrison, D.S. Geller, J.D. Gill, V.O. Lewis, R. Gorlick, Current and future therapeutic approaches for osteosarcoma, *Expert Rev Anticancer Ther*, 18 (2018) 39-50.
- [6] N. Jaffe, O.S. Bruland, S.S. Bielack, *Pediatric and Adolescent Osteosarcoma*, Springer, Boston, MA, 2010.
- [7] B.A. Lindsey, J.E. Markel, E.S. Kleinerman, Osteosarcoma Overview, *Rheumatol Ther*, 4 (2017) 25-43.
- [8] S. Mehnath, V. Muthuraj, M. Jeyaraj, Biomimetic and osteogenic natural HAP coated three dimensional implant for orthopaedic application, *Eur Polym J*, 175 (2022) 111387.
- [9] M. Arjama, S. Mehnath, M. Rajan, M. Jeyaraj, Injectable cuttlefish HAP and macromolecular fibroin protein hydrogel for natural bone mimicking matrix for enhancement of osteoinduction progression, *Reactive and Functional Polymers*, 160 (2021) 104841.
- [10] S. Mehnath, M. Arjama, M. Rajan, K. Premkumar, K. Karthikeyan, M. Jeyaraj, Mineralization of bioactive marine sponge and electrophoretic deposition on Ti-6Al-4V implant for osteointegration, *Surface and Coatings Technology*, 392 (2020) 125727.
- [11] F. Kurtuldu, N. Mutlu, A.R. Boccaccini, D. Galusek, Gallium containing bioactive materials: A review of anticancer, antibacterial, and osteogenic properties, *Bioactive Materials*, 17 (2022) 125-146.
- [12] K.S. Rana, L.P.d. Souza, M.A. Isaacs, F.N.S. Raja, A.P. Morrell, R.A. Martin, Development and Characterization of Gallium-Doped Bioactive Glasses for Potential Bone Cancer Applications, *ACS Biomaterials Science & Engineering*, 3 (2017) 3425-3432.
- [13] J.H. Lopes, A. Magalha, C.A. Bertran, Morphological, structural, and in vitro bioactivity of core-shell-structured bioactive glass by multitechnical spectroscopic approach, *Ceram Int*, 48 (2022) 8039-8050.
- [14] F.V. Ferreira, C.G. Otoni, J.H. Lopes, L.P. de Souza, L.H.I. Mei, L.M.F. Lona, K. Lozano, A.O. Lobo, L.H.C. Mattoso, Ultrathin polymer fibers hybridized with bioactive ceramics: A review on fundamental pathways of electrospinning towards bone regeneration, *Mater Sci Eng C Mater Biol Appl*, 123 (2021) 111853.
- [15] R.A. Martin, S. Yue, J.V. Hanna, P.D. Lee, R.J. Newport, M.E. Smith, J.R. Jones, Characterizing the hierarchical structures of bioactive sol-gel silicate glass and hybrid scaffolds for bone regeneration, *Philos T R Soc A*, 370 (2012) 1422-1443.
- [16] Y. Wang, H. Pan, X. Chen, The Preparation of Hollow Mesoporous Bioglass Nanoparticles With Excellent Drug Delivery Capacity for Bone Tissue Regeneration, *Front Chem*, 7 (2019) 283.
- [17] S. Mehnath, K. Karthikeyan, M. Rajan, M. Jeyaraj, Fabrication of bone-targeting hyaluronic acid coupled alendronate-bioactive glass for osteosarcoma therapy, *Mater Chem Phys*, 273 (2021) 125146.
- [18] J.H. Lopes, L.P. Souza, J.A. Domingues, F.V. Ferreira, M. de Alencar Hausen, J.A. Camilli, R.A. Martin, E.A. de Rezende Duek, I.O. Mazali, C.A. Bertran, In vitro and in vivo osteogenic potential of niobium-doped 45S5 bioactive glass: A comparative study, *Journal of biomedical materials research. Part B, Applied biomaterials*, 108 (2020) 1372-1387.

- [19] L.P.L. de Souza, J.H. Lopes, F.V. Ferreira, R.A. Martin, C.A. Bertran, J.A. Camilli, Evaluation of effectiveness of 45S5 bioglass doped with niobium for repairing critical-sized bone defect in in vitro and in vivo models, *J Biomed Mater Res A*, 108 (2020) 446-457.
- [20] L. Souza, J.H. Lopes, D. Encarnacao, I.O. Mazali, R.A. Martin, J.A. Camilli, C.A. Bertran, Comprehensive in vitro and in vivo studies of novel melt-derived Nb-substituted 45S5 bioglass reveal its enhanced bioactive properties for bone healing, *Sci Rep*, 8 (2018) 12808.
- [21] J.H. Lopes, A. Magalhães, I.O. Mazali, C.A. Bertran, H.E. Kim, Effect of Niobium Oxide on the Structure and Properties of Melt-Derived Bioactive Glasses, *Journal of the American Ceramic Society*, 97 (2014) 3843-3852.
- [22] T. Miyazaki, H.M. Kim, T. Kokubo, C. Ohtsuki, T. Nakamura, Apatite-forming ability of niobium oxide gels in a simulated body fluid, *J Ceram Soc Jpn*, 109 (2001) 929-933.
- [23] J.H. Lopes, L.P. Souza, J.A. Domingues, F.V. Ferreira, M. de Alencar Hausen, J.A. Camilli, R.A. Martin, E.A. de Rezende Duek, I.O. Mazali, C.A. Bertran, In vitro and in vivo osteogenic potential of niobium-doped 45S5 bioactive glass: A comparative study, *Journal of biomedical materials research. Part B, Applied biomaterials*, (2019).
- [24] L.P.L. de Souza, J.H. Lopes, F.V. Ferreira, R.A. Martin, C.A. Bertran, J.A. Camilli, Evaluation of effectiveness of 45S5 bioglass doped with niobium for repairing critical-sized bone defect in in vitro and in vivo models, *J Biomed Mater Res A*, (2019).
- [25] M.M. Hart, R.H. Adamson, Antitumor activity and toxicity of salts of inorganic group 3a metals: aluminum, gallium, indium, and thallium, *Proc Natl Acad Sci U S A*, 68 (1971) 1623-1626.
- [26] Y. Kaneko, M. Thoendel, O. Olakanmi, B.E. Britigan, P.K. Singh, The transition metal gallium disrupts *Pseudomonas aeruginosa* iron metabolism and has antimicrobial and antibiofilm activity, *J Clin Invest*, 117 (2007) 877-888.
- [27] L.P.L. de Souza, F.V. Ferreira, J.H. Lopes, J.A. Camilli, R.A. Martin, Cancer Inhibition and In Vivo Osteointegration and Compatibility of Gallium-Doped Bioactive Glasses for Osteosarcoma Applications, *ACS applied materials & interfaces*, 01 (2022) 446-457.
- [28] B. Kubista, T. Schoefl, L. Mayr, S. van Schoonhoven, P. Heffeter, R. Windhager, B.K. Keppler, W. Berger, Distinct activity of the bone-targeted gallium compound KP46 against osteosarcoma cells - synergism with autophagy inhibition, *J Exp Clin Cancer Res*, 36 (2017) 52.
- [29] A. Rahimnejad Yazdi, L. Torkan, W. Stone, M.R. Towler, The impact of gallium content on degradation, bioactivity, and antibacterial potency of zinc borate bioactive glass, *Journal of biomedical materials research. Part B, Applied biomaterials*, 106 (2018) 367-376.
- [30] G. Malavasi, A. Pedone, M.C. Menziani, Study of the Structural Role of Gallium and Aluminum in 45S5 Bioactive Glasses by Molecular Dynamics Simulations, *The Journal of Physical Chemistry B*, 117 (2013) 4142-4150.
- [31] O.M.V.M. Bueno, C.L. Herrera, C.A. Bertran, M.A. San-Miguel, J.H. Lopes, An experimental and theoretical approach on stability towards hydrolysis of triethyl phosphate and its effects on the microstructure of sol-gel-derived bioactive silicate glass, *Materials Science and Engineering: C*, 120 (2021) 111759.
- [32] J.H. Lopes, O. Bueno, I.O. Mazali, C.A. Bertran, Investigation of citric acid-assisted sol-gel synthesis coupled to the self-propagating combustion method for preparing bioactive glass with high structural homogeneity, *Mater Sci Eng C Mater Biol Appl*, 97 (2019) 669-678.
- [33] G.S. Balbinot, F.M. Collares, F. Visioli, P.B.F. Soares, A.S. Takimi, S.M.W. Samuel, V.C.B. Leitune, Niobium addition to sol-gel derived bioactive glass powders and scaffolds: In vitro

characterization and effect on pre-osteoblastic cell behavior, *Dental materials* : official publication of the Academy of Dental Materials, 34 (2018) 1449-1458.

[34] S. Shruti, A.J. Salinas, G. Malavasi, G. Lusvardi, L. Menabue, C. Ferrara, P. Mustarelli, M. Vallet-Regi, Structural and in vitro study of cerium, gallium and zinc containing sol-gel bioactive glasses, *Journal of Materials Chemistry*, 22 (2012) 13698-13706.

[35] J.H. Lopes, C.G. Franca, M.M. Beppu, Development and characterization of membranes derived from SF/GLY/58S hybrid xerogels for the release of inorganic ions as an osteogenic stimulus for bone regeneration, *Eur Polym J*, 116 (2019) 425-437.

[36] F.A. Moustafa, M. Abdel-Baki, A.M. Fayad, F. El-Diasty, Role of Mixed Valence Effect and Orbital Hybridization on Molar Volume of Heavy Metal Glass for Ionic Conduction Pathways Augmentation, *American Journal of Materials Science*, 4 (2014) 119-126.

[37] A. Doostmohammadi, A. Monshi, R. Salehi, M.H. Fathi, Z. Golniya, A.U. Daniels, Bioactive glass nanoparticles with negative zeta potential, *Ceram Int*, 37 (2011) 2311-2316.

[38] M. Cerruti, D. Greenspan, K. Powers, Effect of pH and ionic strength on the reactivity of Bioglass 45S5, *Biomaterials*, 26 (2005) 1665-1674.

[39] L.T. Zhuravlev, The surface chemistry of amorphous silica. Zhuravlev model, *Colloid Surface A*, 173 (2000) 1-38.

[40] H. Aguiar, J. Serra, P. Gonzalez, B. Leon, Structural study of sol-gel silicate glasses by IR and Raman spectroscopies, *Journal of Non-Crystalline Solids*, 355 (2009) 475-480.

[41] A. Aronne, V.N. Sigaev, B. Champagnon, E. Fanelli, V. Califano, L.Z. Usmanova, P. Pernice, The origin of nanostructuring in potassium niobosilicate glasses by Raman and FTIR spectroscopy, *Journal of Non-Crystalline Solids*, 351 (2005) 3610-3618.

[42] L. Lefebvre, J. Chevalier, L. Gremillard, R. Zenati, G. Thollet, D. Bernache-Assolant, A. Govin, Structural transformations of bioactive glass 45S5 with thermal treatments, *Acta Mater*, 55 (2007) 3305-3313.

[43] K. Lin, C. Lin, Y. Zeng, High mechanical strength bioactive wollastonite bioceramics sintered from nanofibers, *RSC Advances*, 6 (2016) 13867-13872.

[44] I. Cacciotti, M. Lombardi, A. Bianco, A. Ravaglioli, L. Montanaro, Sol-gel derived 45S5 bioglass: synthesis, microstructural evolution and thermal behaviour, *J Mater Sci Mater Med*, 23 (2012) 1849-1866.

[45] K.C. Mathai, S. Vidya, A. John, S. Solomon, J.K. Thomas, Structural, Optical, and Compactness Characteristics of Nanocrystalline CaNb₂O₆ Synthesized through an Autoigniting Combustion Method, *Advances in Condensed Matter Physics*, 2014 (2014) 735878.

[46] C.C. Lin, L.C. Huang, P.Y. Shen, Na₂CaSi₂O₆-P₂O₅ based bioactive glasses. Part 1: Elasticity and structure, *Journal of Non-Crystalline Solids*, 351 (2005) 3195-3203.

[47] B. Samuneva, S. Kralchev, V. Dimitrov, Structure and optical properties of niobium silicate glasses, *Journal of Non-Crystalline Solids*, 129 (1991) 54-63.

[48] L.F. Santos, L. Wondraczek, J. Deubener, R.M. Almeida, Vibrational spectroscopy study of niobium germanosilicate glasses, *Journal of Non-Crystalline Solids*, 353 (2007) 1875-1881.

[49] N.A. Sharaf, R.A. Condrate Sr, A.A. Ahmed, FTIR spectral/structural investigation of the ion exchange/thermal treatment of silver ions into a silicate glass, *Materials Letters*, 11 (1991) 115-118.

[50] N. Gomez-Cerezo, E. Verron, V. Montouillout, F. Fayon, P. Lagadec, J.M. Bouler, B. Bujoli, D. Arcos, M. Vallet-Regi, The response of pre-osteoblasts and osteoclasts to gallium containing mesoporous bioactive glasses, *Acta biomaterialia*, 76 (2018) 333-343.

- [51] F.D. Hardcastle, I.E. Wachs, Determination of niobium-oxygen bond distances and bond orders by Raman spectroscopy, *Solid State Ionics*, 45 (1991) 201-213.
- [52] P.L. Higby, J.E. Shelby, J.C. Phillips, A.D. Legrand, EXAFS study of alkali galliosilicate glasses, *Journal of Non-Crystalline Solids*, 105 (1988) 139-148.
- [53] M. Okuno, F. Marumo, T. Sakamaki, S. Hosoya, M. Miyake, The structure analyses of NaGaSi₃O₈, NaAlGe₃O₈ and NaGaGe₃O₈ glasses by X-ray diffraction and EXAFS measurements, *Mineralogical Journal*, 12 (1984) 101-121.
- [54] Y. Zhao, R.L. Frost, Raman spectroscopy and characterisation of α -gallium oxyhydroxide and β -gallium oxide nanorods, *J Raman Spectrosc*, 39 (2008) 1494-1501.
- [55] D. Dohy, G. Lucazeau, Valence force field and raman spectra of β Ga₂O₃, *Journal of Molecular Structure*, 79 (1982) 419-422.
- [56] J.H. Lopes, Biovidros derivados do 45S5: Os efeitos do Nb₂O₅ ou da modificação da superfície com Ca²⁺ sobre a estrutura e bioatividade, in: Universidade Estadual de Campinas - Instituto de Química, UNICAMP, Campinas, 2015.
- [57] J.P. Thielemann, F. Girgsdies, R. Schlögl, C. Hess, Pore structure and surface area of silica SBA-15: influence of washing and scale-up, *Beilstein journal of nanotechnology*, 2 (2011) 110-118.
- [58] N. Gupta, D. Santhiya, Mesoporous bioactive glass and its applications, in: H. Ylänen (Ed.) *Bioactive Glasses*, Woodhead Publishing, 2018, pp. 63-85.
- [59] C.T. Wu, J. Chang, Multifunctional mesoporous bioactive glasses for effective delivery of therapeutic ions and drug/growth factors, *Journal of Controlled Release*, 193 (2014) 282-295.
- [60] C.T. Wu, J. Chang, Mesoporous bioactive glasses: structure characteristics, drug/growth factor delivery and bone regeneration application, *Interface Focus*, 2 (2012) 292-306.
- [61] B. Sui, G. Zhong, J. Sun, Drug-loadable Mesoporous Bioactive Glass Nanospheres: Biodistribution, Clearance, BRL Cellular Location and Systemic Risk Assessment via ⁴⁵Ca Labelling and Histological Analysis, 6 (2016) 33443.
- [62] R.G. Hill, D.S. Brauer, Predicting the bioactivity of glasses using the network connectivity or split network models, *Journal of Non-Crystalline Solids*, 357 (2011) 3884-3887.
- [63] J.E. Shelby, Introduction to glass science and technology, in, Royal Society of Chemistry, Cambridge, 2005.
- [64] L.L. Hench, R.J. Splinter, W.C. Allen, T.K. Greenlee, Bonding mechanisms at the interface of ceramic prosthetic materials, *Journal of Biomedical Materials Research*, 5 (1971) 117-141.
- [65] A. Tilocca, A.N. Cormack, Exploring the Surface of Bioactive Glasses: Water Adsorption and Reactivity, *The Journal of Physical Chemistry C*, 112 (2008) 11936-11945.
- [66] A. Tilocca, Sodium migration pathways in multicomponent silicate glasses: Car-Parrinello molecular dynamics simulations, *J Chem Phys*, 133 (2010) 014701.
- [67] P. Xu, H. Wang, R. Tong, Q. Du, W. Zhong, Preparation and morphology of SiO₂/PMMA nanohybrids by microemulsion polymerization, *Colloid and Polymer Science*, 284 (2006) 755-762.
- [68] J.H. Lopes, E.M.B. Fonseca, I.O. Mazali, A. Magalhaes, R. Landers, C.A. Bertran, Facile and innovative method for bioglass surface modification: Optimization studies, *Mater Sci Eng C Mater Biol Appl*, 72 (2017) 86-97.
- [69] J.H. Lopes, I.O. Mazali, R. Landers, C.A. Bertran, H.E. Kim, Structural Investigation of the Surface of Bioglass 45S5 Enriched with Calcium Ions, *Journal of the American Ceramic Society*, 96 (2013) 1464-1469.

- [70] R. Smeets, A. Kolk, M. Gerressen, O. Driemel, O. Maciejewski, B. Hermanns-Sachweh, D. Riediger, J.M. Stein, A new biphasic osteoinductive calcium composite material with a negative Zeta potential for bone augmentation, *Head Face Med*, 5 (2009) 13.
- [71] F.V. Ferreira, L.P. Souza, T.M.M. Martins, J.H. Lopes, B.D. Mattos, M. Mariano, I.F. Pinheiro, T.M. Valverde, S. Livi, J.A. Camilli, A.M. Goes, R.F. Gouveia, L.M.F. Lona, O.J. Rojas, Nanocellulose/bioactive glass cryogels as scaffolds for bone regeneration, *Nanoscale*, 11 (2019) 19842-19849.